An improved lattice measurement
of the critical coupling in ϕ_2^4 theory

David Schaich[1,2,*] and Will Loinaz[2,†]

[1]*Department of Physics and Center for Computational Science,*
Boston University, Boston, MA 02215

[2]*Department of Physics, Amherst College, Amherst, MA 01002*

(Dated: 30 January 2009)

Abstract

We use Monte Carlo simulations to obtain an improved lattice measurement of the critical coupling constant $\left[\lambda/\mu^2\right]_{crit}$ for the continuum $(1 + 1)$-dimensional $(\lambda/4)\phi^4$ theory. We find that the critical coupling constant depends logarithmically on the lattice coupling, resulting in a continuum value of $\left[\lambda/\mu^2\right]_{crit} = 10.8^{+.10}_{-.05}$, in considerable disagreement with the previously reported $\left[\lambda/\mu^2\right]_{crit} = 10.26^{+.08}_{-.04}$. Although this logarithmic behavior was not observed in earlier lattice studies, it is consistent with them, and expected analytically.

*Electronic address: schaich@physics.bu.edu

†Electronic address: waloinaz@amherst.edu

1

I. INTRODUCTION

The two-dimensional ϕ_2^4 field theory specified by the Euclidean Lagrangian

$$\mathcal{L}_E = \frac{1}{2}(\nabla\phi)^2 + \frac{1}{2}\mu_0^2\phi^2 + \frac{\lambda}{4}\phi^4 \tag{1}$$

exhibits a phase transition between a symmetric phase with $\langle\phi\rangle = 0$ and a phase in which the discrete symmetry of the Lagrangian under $\phi \to -\phi$ is broken [1, 2]. Loinaz and Willey [3] have used Monte Carlo simulations to calculate the critical value of the coupling constant that separates the two phases of the theory.

In this work we perform similar calculations, discretizing the Euclidean quantum field theory (EQFT) of Eqn. 1 in terms of the two dimensionless lattice parameters

$$\hat{\lambda} \equiv \lambda a^2 \qquad\qquad \hat{\mu}_0^2 \equiv \mu_0^2 a^2, \tag{2}$$

where $a > 0$ is the lattice spacing. (In two dimensions, both λ and μ_0^2 have mass dimension $[\lambda] = [\mu_0^2] = 2$.) The lattice action that regularizes Eqn. 1 is

$$\mathcal{A} = \sum_n \left[\frac{1}{2}\sum_{\nu=1}^d (\phi_{n+e_\nu} - \phi_n)^2 + \frac{1}{2}\hat{\mu}_0^2\phi_n^2 + \frac{\hat{\lambda}}{4}\phi_n^4 \right], \tag{3}$$

where e_ν is the unit vector in the ν direction. The EQFT is the continuum limit $a \to 0$ of this lattice model.

In two dimensions, the field strength and self-coupling renormalization factors Z_ϕ and Z_λ are finite, and do not affect the phase structure of the theory. However, there is an infinite mass renormalization, which requires that the bare mass parameter be tuned to infinity as the continuum limit is taken, $\mu_0^2 \sim \mu^2 \ln(1/a)$, where μ^2 is the finite renormalized mass squared. Since λ is independent of a and μ_0^2 diverges only logarithmically as $a \to 0$, both $\hat{\lambda}$ and $\hat{\mu}_0^2$ vanish in the continuum limit $a \to 0$. Taking the continuum limit therefore reduces the number of independent dimensionless parameters from two to one, which we take to be the dimensionless coupling constant $f = \lambda/\mu^2$.

We can parametrize the mass renormalization as

$$\mu_0^2 = \mu^2 - \delta\mu^2, \tag{4}$$

$$\mathcal{L}_E = \frac{1}{2}(\nabla\phi)^2 + \frac{1}{2}\mu^2\phi^2 + \frac{\lambda}{4}\phi^4 - \frac{1}{2}\delta\mu^2\phi^2, \tag{5}$$

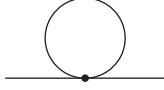FIG. 1: The only divergent Feynman diagram in ϕ_2^4 theory.

where μ^2 and the finite part of $\delta\mu^2$ depend on the choice of renormalization condition. We want to choose a renormalization scheme in which the effective coupling constant f distinguishes between the two phases of the theory, which is not the case for several popular renormalization conditions [3]. We will achieve this by choosing the mass renormalization to be equivalent to normal-ordering the interaction in the interaction picture in the symmetry phase.

There is only one divergent Feynman diagram in ϕ_2^4 theory, Fig. 1, which involves the integral

$$
\begin{aligned}
A_{\mu^2} &= \frac{1}{N^2}\sum_{k_1=1}^{N}\sum_{k_2=1}^{N}\frac{1}{\hat{\mu}^2 + 4\sin^2(\pi k_1/N) + 4\sin^2(\pi k_2/N)} \\
&\to \int\frac{d^2p}{(2\pi)^2}\frac{1}{p^2+\mu^2}
\end{aligned}
\tag{6}
$$

in the continuum limit. From Eqns. 1 and 4,

$$
G^{-1}(p^2) = p^2 + \mu_0^2 + \Sigma_0(p^2) = p^2 + \mu^2 + \Sigma(p^2),
\tag{7}
$$

$$
\Sigma(p^2) = 3\lambda A_{\mu^2} - \delta\mu^2 + \text{two-loop}.
\tag{8}
$$

Therefore the renormalization condition

$$
\delta\mu^2 = 3\lambda A_{\mu^2}
\tag{9}
$$

removes all ultraviolet divergence from the perturbation series based on the renormalized parametrization of Eqn. 4.

Applying this renormalization condition,

$$
\begin{aligned}
\mathcal{L}_E &= \frac{1}{2}(\nabla\phi)^2 + \frac{1}{2}\mu^2\phi^2 + \frac{\lambda}{4}\phi^4 - \frac{3}{2}\lambda A_{\mu^2}\phi^2 \\
&= \frac{1}{2}(\nabla\phi)^2 + \frac{1}{2}\mu^2\phi^2 + \frac{\lambda}{4}{:}\phi^4{:}_{\mu^2},
\end{aligned}
\tag{10}
$$

dropping a constant piece in the second line. In terms of $f = \lambda/\mu^2$, the first line of Eqn. 10 can be written as

$$
\mathcal{L}_E = \frac{1}{2}(\nabla\phi)^2 + \frac{1}{2}\mu^2(1 - 3fA_{\mu^2})\phi^2 + \frac{f\mu^2}{4}\phi^4.
\tag{11}
$$

On the lattice ($a > 0$), A_{μ^2} is finite, so we can argue that for f sufficiently small, the exact effective potential has a single minimum at $\langle\phi\rangle = 0$. The coefficient of ϕ^2 in Eqn. 11 is negative for large f, suggesting a transition to the broken symmetry phase. However, the effective potential need not be well approximated by its tree-level form at strong coupling. Chang [1] has shown that this transition does occur, using a duality transformation from the strong coupling regime of Eqn. 11 to a weakly-coupled theory normal-ordered with respect to the vacuum of the broken symmetry phase.

We proceed by using Monte Carlo simulations to map the critical line in the $(\hat{\mu}_0^2, \hat{\lambda})$ plane. We determine critical values of $\hat{\mu}_{0c}^2(\hat{\lambda})$ for various $\hat{\lambda}$, calculating the infinite-lattice-size limit of Monte Carlo data measured on lattices of finite size. We then impose our renormalization condition

$$\hat{\mu}^2 = \hat{\mu}_0^2 + 3\hat{\lambda}A_{\mu^2} \qquad (12)$$

using the integral representation of A_{μ^2} in the infinite-volume limit,

$$A_{\mu^2} = \int_0^\infty dt \exp\left[-\hat{\mu}^2 t\right] \left(\exp(-2t)I_0(2t)\right)^2. \qquad (13)$$

Here I_0 is a modified Bessel function of the first kind.

For fixed $\hat{\lambda} \neq 0$, we solve Eqns. 12 and 13 numerically to determine $\hat{\mu}_c^2$ from $\hat{\mu}_{0c}^2$. We then extrapolate $\hat{\lambda} \to 0$ to obtain the critical coupling constant

$$\left[\lambda/\mu^2\right]_{crit} \equiv f_c = \lim_{\hat{\lambda},\hat{\mu}^2 \to 0} \left[\hat{\lambda}/\hat{\mu}_c^2\right] \qquad (14)$$

in the continuum limit. We will see that this extrapolation has a nonlinear form.

II.   SIMULATIONS

We performed Monte Carlo simulations based on the lattice action of Eqn. 3 on $N \times N$ lattices with $N = 32, 64, 128, 256, 512$, and 1024. For each N, we set $\hat{\lambda} = 1.0, 0.7, 0.5, 0.25,$ $0.1, 0.05, 0.03, 0.02$, and 0.01, and for each $(N, \hat{\lambda})$ scanned in $\hat{\mu}_0^2$ beginning in the symmetric phase and ending in the broken symmetry phase. To further constrain the data at small $\hat{\lambda}$, we performed additional simulations at $N = 600$ and 1200 for $\hat{\lambda} = 0.05, 0.03, 0.02$, and 0.01.

To reduce critical slowing down, our simulations execute a Wolff cluster algorithm [4] update on the embedded Ising model after every five random sweeps of the lattice with standard

Metropolis updating, as in [3, 5]. After an initial thermalization of 2^{13}-2^{14} Metropolis-Wolff cycles, we measured lattice quantities following each of an additional 2^{13}-2^{14} cycles.

Since these measurements are not independent, we also calculated the autocorrelation time τ for each $(N, \hat{\lambda}, \hat{\mu}_0^2)$ simulation and incorporated it into our analysis. Typical autocorrelation times are around ten measurements, with maximum autocorrelation times around 100 measurements for $\hat{\lambda} \ll 1$ on small lattices. In every simulation the thermalization time exceeded 100τ and we took at least 100 statistically independent measurements. As a result, our statistical uncertainties are quite small in comparison to systematic uncertainties.

We use three diagnostics to determine the critical value of $\hat{\mu}_{0c}^2$ where the phase transition occurs for fixed $\hat{\lambda}$. The first is the familiar peak in the susceptibility $\chi \propto \langle \phi^2 \rangle - \langle |\phi| \rangle^2$, with uncertainty extracted from the full width of the peak at half its maximum value (FWHM).

The second diagnostic is the bimodality $B(\hat{\mu}_0^2)$, a parameterization of the shape of the histogram of the values of ϕ measured during each simulation with fixed $(N, \hat{\lambda}, \hat{\mu}_0^2)$ [3]. Fig. 2 illustrates these histograms in the two phases of ϕ_2^4 theory: in the symmetric phase the histogram has a single peak around $\langle \phi \rangle = 0$, while in the broken symmetry phase it has two peaks, around $\pm \langle |\phi| \rangle \neq 0$. Constructing the histogram with an odd number of bins, we define the bimodality as

$$B = 1 - \frac{n_0}{n_{max}}, \tag{15}$$

where n_0 is the number of measurements in the central bin around zero, and n_{max} is the largest number in any bin. In the symmetric phase, $B \ll 1$, while in the broken symmetry phase $B \approx 1$ (cf. Fig. 2).

Since B depends on the specific evolution of the system, it can vary considerably for similar values of $\hat{\mu}_0^2$, particularly in the symmetric phase. To smooth out this jitter, we consider the three-point running average $\widetilde{B}(\hat{\mu}_0^2)$ of $B(\hat{\mu}_0^2)$ over $\hat{\mu}_0^2$,

$$\widetilde{B}(\hat{\mu}_0^2) = \left[B(\hat{\mu}_0^2 - \Delta\hat{\mu}_0^2) + B(\hat{\mu}_0^2) + B(\hat{\mu}_0^2 + \Delta\hat{\mu}_0^2) \right]/3. \tag{16}$$

Fig. 3 illustrates the benefits of this smoothing procedure. We take as the phase transition point the value of $\hat{\mu}_0^2$ for which $\widetilde{B}(\hat{\mu}_0^2)$ is closest to 0.5, with bounds given by the $\hat{\mu}_0^2$ most distant from this critical $\hat{\mu}_{0c}^2$ for which $0.1 < \widetilde{B} < 0.95$ (cf. Fig. 3). These conventions produce results consistent with those from the susceptibility, with comparable (though generally smaller) uncertainties, as shown in Table I.
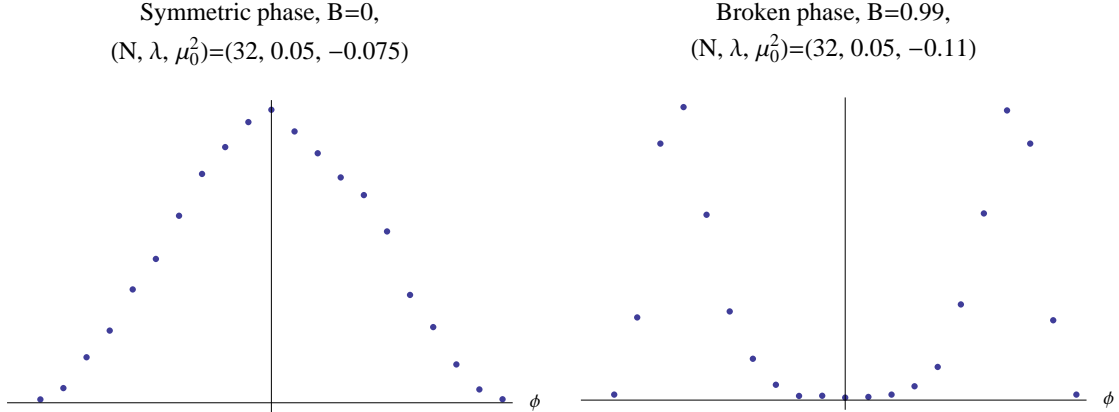
Symmetric phase, B=0,
(N, λ, μ_0^2)=(32, 0.05, −0.075)

Broken phase, B=0.99,
(N, λ, μ_0^2)=(32, 0.05, −0.11)

FIG. 2: Histograms of ϕ for simulations with $N = 32$ and $\hat{\lambda} = 0.05$, in the symmetric phase (left, $\hat{\mu}_0^2 = -0.075$) and broken symmetry phase (right, $\hat{\mu}_0^2 = -0.11$).

Raw Bimodality, (N, λ)=(64, 0.5)
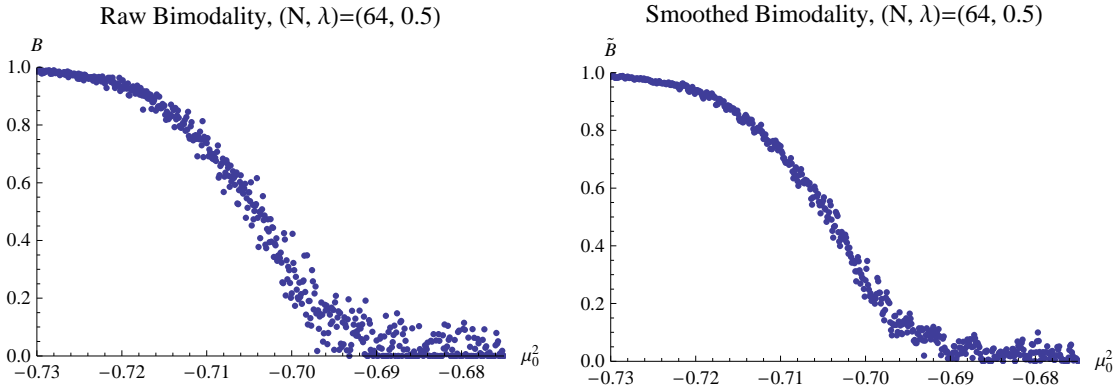
Smoothed Bimodality, (N, λ)=(64, 0.5)

FIG. 3: Bimodality plotted against $\hat{\mu}_0^2$ for simulations with $N = 64$ and $\hat{\lambda} = 0.5$, before (left) and after (right) smoothing.

To verify that the bimodality is a robust indicator of the phase transition, we checked its behavior in the well-understood two-dimensional Ising model. Using the conventions stated above, we found that the critical $\hat{\mu}_{0c}^2$ indicated by the bimodality agrees well with that indicated by the susceptibility in this case as well, with comparable uncertainties. Both observables agree with the exact analytic result.

Finally, we extract a third estimate of the critical $\hat{\mu}_{0c}^2$ using the Binder cumulant [6]

$$U = 1 - \frac{\langle\phi^4\rangle}{3\langle\phi^2\rangle^2}. \tag{17}$$

For $\hat{\lambda}$ fixed, U has a fixed point at the critical $\hat{\mu}_{0c}^2$ for any value of the lattice size N. We take as the critical $\hat{\mu}_{0c}^2$ the value of $\hat{\mu}_0^2$ at which U for the three largest N are closest together,

6

TABLE I: Critical $\hat{\mu}_{0c}^2$ from each phase transition indicator.

$\hat{\lambda}$	Susceptibility	Bimodality	Cumulant
1.00	-1.27233(16)	-1.27258(10)	-1.27260(45)
0.70	-0.95151(25)	-0.95152(7)	-0.95180(40)
0.50	-0.72080(11)	-0.72131(9)	-0.72130(30)
0.25	-0.40346(18)	-0.40373(6)	-0.40390(20)
0.10	-0.18424(11)	-0.18432(9)	-0.18430(20)
0.05	-0.10060(5)	-0.10071(4)	-0.10100(35)
0.03	-0.06410(4)	-0.06414(5)	-0.06420(15)
0.02	-0.04464(3)	-0.04468(5)	-0.04500(30)
0.01	-0.02397(6)	-0.02399(5)	-0.02410(10)

with bounds given by the $\hat{\mu}_0^2$ at which all three separate.

This analysis of the cumulant in Eqn. 17 produces a single critical $\hat{\mu}_{0c}^2$ for each $\hat{\lambda}$, while we have susceptibility and bimodality data for each $(N, \hat{\lambda})$. Performing a linear regression to find the $N \to \infty$ limit of the susceptibility and bimodality data with $\hat{\lambda}$ fixed gives us a total of three independent indicators of the critical $\hat{\mu}_{0c}^2$ for each $\hat{\lambda}$.

We find all three values for each $\hat{\lambda}$ consistent with each other, with comparable uncertainties (Table I). Combining them produces the second column in Table II. The third column in Table II holds the corresponding critical renormalized $\hat{\mu}_c^2$ determined from Eqns. 12 and 13, while the fourth presents the values of the critical coupling $\hat{\lambda}/\hat{\mu}_c^2$ which are to be extrapolated to the $a \to 0$ continuum limit.

III. ANALYSIS

Fig. 4 plots the values of $\hat{\lambda}/\hat{\mu}_c^2$ in the fourth column of Table II and clearly rules out a linear $\hat{\lambda} \to 0$ extrapolation like that performed in [3].

Analytic investigations into the structure of scalar field theories, and super-renormalizable theories more generally, long ago established that correlation functions in these theories typically depend on logarithms of the coupling [7, 8, 9, 10, 11]. Jackiw and Templeton [10] explicitly demonstrated the presence of such logarithmic terms in a simple ϕ_4^3 model,

TABLE II: Critical $\hat{\mu}_{0c}^2$, $\hat{\mu}_c^2$ and $\hat{\lambda}/\hat{\mu}_c^2$ for different $\hat{\lambda}$.

$\hat{\lambda}$	$\hat{\mu}_{0c}^2$	$\hat{\mu}_c^2$	$\hat{\lambda}/\hat{\mu}_c^2$
1.00	-1.27251(16)	0.097320(46)	10.275(5)
0.70	-0.95153(16)	0.068462(45)	10.225(7)
0.50	-0.72112(11)	0.048884(32)	10.228(7)
0.25	-0.40372(9)	0.024176(26)	10.341(11)
0.10	-0.18429(8)	0.009476(23)	10.553(26)
0.05	-0.10067(12)	0.004679(33)	10.686(76)
0.03	-0.06412(5)	0.002794(15)	10.737(59)
0.02	-0.04466(10)	0.001870(28)	10.695(163)
0.01	-0.02400(4)	0.000931(12)	10.739(138)
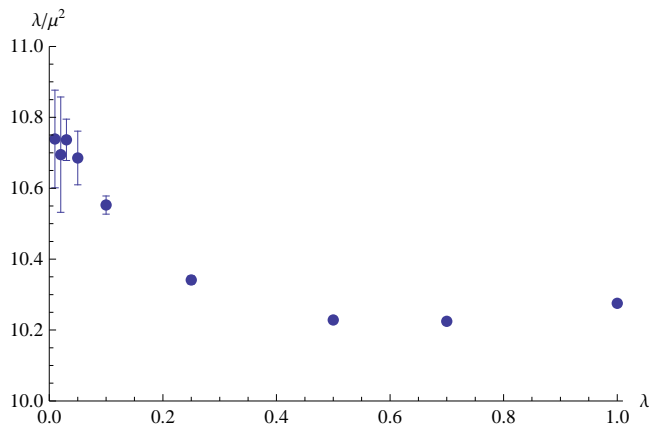
FIG. 4: Critical coupling constant $\hat{\lambda}/\hat{\mu}_c^2$ plotted against $\hat{\lambda}$.

using a truncated Bethe-Salpeter equation. This non-analytic dependence on the coupling appears generically in more complicated super-renormalizable theories as well, including the ϕ_2^4 theory we consider here.

We can numerically investigate the effect of such logarithmic dependence by fitting the data in Table II and Fig. 4 to a function of the form

$$\hat{\lambda}/\hat{\mu}_c^2 = c_0 + c_1\hat{\lambda} + c_2\hat{\lambda}\ln\hat{\lambda}. \tag{18}$$

The constant c_0 is exactly the continuum critical coupling constant f_c we wish to determine. Performing this fit, we find $c_0 = f_c = 10.78(3)$, with $\chi^2 = 1.21$ per degree of freedom (dof).

8

TABLE III: $\hat{\lambda}, \hat{\mu}^2 \to 0$ extrapolations of $\hat{\lambda}/\hat{\mu}_c^2$ vs. $\hat{\lambda}$.

Form of $\hat{\lambda}/\hat{\mu}_c^2$ fit	f_c	χ^2/dof
$f_c + c_1\hat{\lambda}$	10.31(6)	48
$f_c + c_1\hat{\lambda} + c_2\hat{\lambda}^2$	10.60(5)	5.8
$f_c + c_1\hat{\lambda} + c_2\hat{\lambda}\ln\hat{\lambda}$	10.78(3)	1.2
$f_c + c_1\hat{\lambda} + c_2\hat{\lambda}\ln\hat{\lambda} + c_3\hat{\lambda}^2$	10.89(2)	0.16
$f_c + c_1\hat{\lambda} + c_2\hat{\lambda}\ln\hat{\lambda} + c_3\hat{\lambda}^2\ln\hat{\lambda}$	10.87(2)	0.13

Performing fits with additional terms ($c_3\hat{\lambda}^2$ or $c_3\hat{\lambda}^2\ln\hat{\lambda}$) results in even larger $f_c \approx 10.9$ with very small $\chi^2/dof \approx 0.15$ (Table III). Fits that do not include a term logarithmic in $\hat{\lambda}$ are poor, with $\chi^2/dof \gg 1$.

We can check the consistency of these results by fitting $\hat{\mu}_c^2$ as a function of $\hat{\lambda}$ and extracting f_c from the coefficient of the term linear in $\hat{\lambda}$,

$$\hat{\mu}_c^2 = d_0 + \hat{\lambda}/f_c + \mathcal{O}(\hat{\lambda}^2).$$

Fitting

$$\hat{\mu}_c^2 = d_0 + \hat{\lambda}/f_c + d_1\hat{\lambda}^2 + d_2\hat{\lambda}^2\ln\hat{\lambda}, \tag{19}$$

we find $f_c = 10.77(4)$ with $\chi^2/dof = 1.1$. As above, including additional terms in the fit raises f_c while dramatically lowering the χ^2/dof, while fits without any logarithmic term have $\chi^2/dof \gg 1$ (Table IV).

Since $\hat{\mu}_c^2 \to 0$ as $\hat{\lambda} \to 0$, we should find the constant term $d_0 \approx 0$ in these fits, and we can also perform fits with d_0 explicitly set to zero as an additional check. Of the fits listed in Table IV, only that of Eqn. 19 has d_0 vanish within uncertainty, although d_0 is within 2σ of zero for the fit form

$$\hat{\mu}_c^2 = d_0 + \hat{\lambda}/f_c + d_1\hat{\lambda}^2 + d_2\hat{\lambda}^3$$

as well. The value of f_c extracted from the fit

$$\hat{\mu}_c^2 = \hat{\lambda}/f_c + d_1\hat{\lambda}^2 + d_2\hat{\lambda}^2\ln\hat{\lambda}, \tag{20}$$

is $f_c = 10.79(3)$ with $\chi^2/dof = 1.0$, in agreement with the values from Eqns. 18 and 19.

Clearly, systematic errors, particularly the choice of continuum extrapolation form, dominate over statistical errors. Tables III and IV summarize f_c for various linear and nonlinear

TABLE IV: $\hat{\lambda} \to 0$ extrapolations of $\hat{\mu}_c^2$ vs. $\hat{\lambda}$.

Form of $\hat{\mu}_c^2$ fit	f_c	χ^2/dof
$d_0 + \hat{\lambda}/f_c$	10.24(2)	28
$d_0 + \hat{\lambda}/f_c + d_1\hat{\lambda}^2$	10.24(6)	33
$d_0 + \hat{\lambda}/f_c + d_1\hat{\lambda}^2 + d_2\hat{\lambda}^3$	10.55(5)	4.1
$d_0 + \hat{\lambda}/f_c + d_1\hat{\lambda}^2 + d_2\hat{\lambda}^2 \ln\hat{\lambda}$	10.77(4)	1.1
$d_0 + \hat{\lambda}/f_c + d_1\hat{\lambda}^2 + d_2\hat{\lambda}^2 \ln\hat{\lambda} + d_3\hat{\lambda}^3$	10.98(2)	0.04
$d_0 + \hat{\lambda}/f_c + d_1\hat{\lambda}^2 + d_2\hat{\lambda}^2 \ln\hat{\lambda} + d_3\hat{\lambda}^3 \ln\hat{\lambda}$	10.93(2)	0.05
$\hat{\lambda}/f_c$	10.27(2)	47
$\hat{\lambda}/f_c + d_1\hat{\lambda}^2$	10.31(7)	49
$\hat{\lambda}/f_c + d_1\hat{\lambda}^2 + d_2\hat{\lambda}^3$	10.61(5)	5.5
$\hat{\lambda}/f_c + d_1\hat{\lambda}^2 + d_2\hat{\lambda}^2 \ln\hat{\lambda}$	10.79(3)	1.0
$\hat{\lambda}/f_c + d_1\hat{\lambda}^2 + d_2\hat{\lambda}^2 \ln\hat{\lambda} + d_3\hat{\lambda}^3$	10.90(2)	0.18
$\hat{\lambda}/f_c + d_1\hat{\lambda}^2 + d_2\hat{\lambda}^2 \ln\hat{\lambda} + d_3\hat{\lambda}^3 \ln\hat{\lambda}$	10.89(2)	0.14

extrapolations, along with the goodness of the fits, χ^2/dof. Neglecting fits with $\chi^2/dof \gg 1$, we adopt a final result of

$$f_c = 10.8^{+.10}_{-.05} \tag{21}$$

to be consistent with the numbers in Tables III and IV.

IV. DISCUSSION

Since our approach closely parallels that of Loinaz and Willey [3], it is distressing that our final result disagrees so strongly with the $f_c = 10.26^{+.08}_{-.04}$ reported there. However, our individual data points are largely consistent with theirs, as shown in Fig. 5. The disagreement between our final results comes almost entirely from the nonlinear continuum extrapolations discussed above.

Re-analyzing the data in [3], we find (Tables V and VI) that they are consistent with all the nonlinear fits considered in our analysis above. Both linear and nonlinear fits all have $\chi^2/dof \sim 0.5$. While nonlinear extrapolations were not required by the data in [3], by considering only the linear case Loinaz and Willey overlooked significant systematic effects
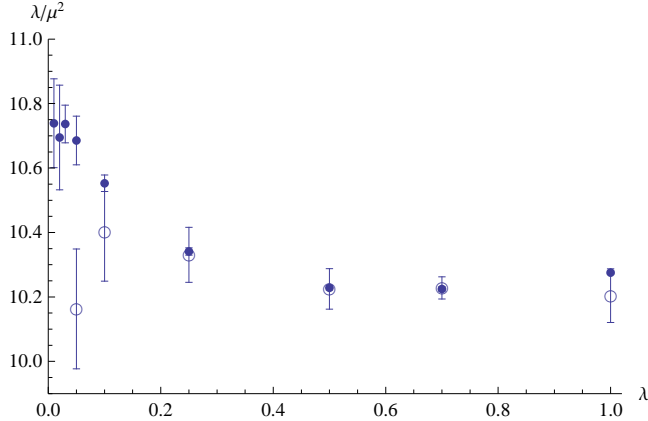
FIG. 5: Our data for $\hat{\lambda}/\hat{\mu}_c^2$ compared with the results of [3] (empty circles).

TABLE V: $\hat{\lambda}, \hat{\mu}^2 \to 0$ extrapolations of $\hat{\lambda}/\hat{\mu}_c^2$ vs. $\hat{\lambda}$, for [3].

Form of $\hat{\lambda}/\hat{\mu}_c^2$ fit	f_c	χ^2/dof
$f_c + c_1\hat{\lambda}$	10.32(5)	0.39
$f_c + c_1\hat{\lambda} + c_2\hat{\lambda}^2$	10.34(9)	0.49
$f_c + c_1\hat{\lambda} + c_2\hat{\lambda}\ln\hat{\lambda}$	10.34(12)	0.51
$f_c + c_1\hat{\lambda} + c_2\hat{\lambda}\ln\hat{\lambda} + c_3\hat{\lambda}^2$	10.18(25)	0.59
$f_c + c_1\hat{\lambda} + c_2\hat{\lambda}\ln\hat{\lambda} + c_3\hat{\lambda}^2\ln\hat{\lambda}$	10.23(22)	0.63

due to fit form. In Tables V and VI, we see $10.2 \lesssim f_c \lesssim 11.9$ in fits with $\chi^2/dof < 1$, consistent with our result $f_c = 10.8^{+.10}_{-.05}$.

Several other authors have also calculated the critical coupling f_c in ϕ_2^4 theory using a variety of methods, numerical schemes, and analytic approximations. These approaches, summarized in Table VII, produce a large spread of results, of which ours is the largest.

The density matrix renormalization group result $f_c = 9.982(2)$ [16] is notable for its extremely small claimed uncertainty. However, this result relies on linear $\hat{\lambda} \to 0$ extrapolations like those in [3], performed with just two data points at $\hat{\lambda} = 0.1, 0.25$, for fixed lattice size $N = 500$ or 1000. A linear $1/N \to 0$ extrapolation is then performed using the two resulting values. Thus, we expect this result to suffer from the difficulties discussed above.

The diffusion Monte Carlo result $f_c = 10 \pm 0.8 \pm 0.4$ [15] agrees with our result within its relatively large statistical and systematic uncertainties. The Gaussian effective potential results $f_c = 10.272$ [12], $f_c = 10.211$ [1], and $f_c = 10.21$ [13] (the last of which coincides

TABLE VI: $\hat{\lambda} \to 0$ extrapolations of $\hat{\mu}_c^2$ vs. $\hat{\lambda}$, for [3].

Form of $\hat{\mu}_c^2$ fit	f_c	χ^2/dof
$d_0 + \hat{\lambda}/f_c$	10.23(3)	0.65
$d_0 + \hat{\lambda}/f_c + d_1\hat{\lambda}^2$	10.37(9)	0.44
$d_0 + \hat{\lambda}/f_c + d_1\hat{\lambda}^2 + d_2\hat{\lambda}^3$	10.57(16)	0.32
$d_0 + \hat{\lambda}/f_c + d_1\hat{\lambda}^2 + d_2\hat{\lambda}^2 \ln \hat{\lambda}$	10.80(24)	0.23
$d_0 + \hat{\lambda}/f_c + d_1\hat{\lambda}^2 + d_2\hat{\lambda}^2 \ln \hat{\lambda} + d_3\hat{\lambda}^3$	11.86(23)	0.02
$d_0 + \hat{\lambda}/f_c + d_1\hat{\lambda}^2 + d_2\hat{\lambda}^2 \ln \hat{\lambda} + d_3\hat{\lambda}^3 \ln \hat{\lambda}$	11.64(12)	0.01
$\hat{\lambda}/f_c$	10.24(2)	0.57
$\hat{\lambda}/f_c + d_1\hat{\lambda}^2$	10.32(5)	0.38
$\hat{\lambda}/f_c + d_1\hat{\lambda}^2 + d_2\hat{\lambda}^3$	10.35(9)	0.49
$\hat{\lambda}/f_c + d_1\hat{\lambda}^2 + d_2\hat{\lambda}^2 \ln \hat{\lambda}$	10.35(12)	0.50
$\hat{\lambda}/f_c + d_1\hat{\lambda}^2 + d_2\hat{\lambda}^2 \ln \hat{\lambda} + d_3\hat{\lambda}^3$	10.19(25)	0.59
$\hat{\lambda}/f_c + d_1\hat{\lambda}^2 + d_2\hat{\lambda}^2 \ln \hat{\lambda} + d_3\hat{\lambda}^3 \ln \hat{\lambda}$	10.24(22)	0.63

with the oscillator representation result) are the next closest. Both the Gaussian effective potential and oscillator representation methods incorrectly predict a first-order phase transition, in violation of the Simon-Griffiths theorem [24], which requires the ϕ_2^4 theory phase transition to be second order.

V. CONCLUSIONS

We have used Monte Carlo simulations to obtain an accurate lattice measurement of the continuum critical coupling constant $f_c = 10.8^{+.10}_{-.05}$ in ϕ_2^4 theory, improving the previously reported Monte Carlo result [3].

While our data are consistent with those reported in [3], our improved precision forces a nonlinear extrapolation to the continuum limit, producing a significantly different continuum result. The older data are compatible with these nonlinear extrapolations, although such nonlinearity was neither required nor investigated previously. Applying nonlinear extrapolations to the older data, we obtain continuum results consistent with our own.

Significantly, nonlinearity – in particular terms logarithmic in the lattice coupling $\hat{\lambda}$ –

TABLE VII: Various results for the critical coupling f_c.

Method	Result	Reference
Monte Carlo	$10.8^{+.10}_{-.05}$	This work
Gaussian effective potential	10.272	[12]
Gaussian effective potential	10.211	[1]
GEP and oscillator rep.	10.21	[13]
Spherical field theory	10.05	[14]
Diffusion Monte Carlo	$10 \pm 0.8 \pm 0.4$	[15]
Density matrix RG	9.982(2)	[16]
Continuum light-front	9.91	[17]
Connected Green function	9.784	[12]
Coupled cluster expansion	$3.80 < f_c < 8.60$	[18]
Discretized light-front	7.325, 7.71	[19]
Discretized light-front	7.316, 5.500	[20, 21]
Random phase approximation	7.2	[22]
Non-Gaussian variational	6.88	[23]

is expected analytically. This convergence of analytic theory and numerical data provides additional evidence that our improved result is accurate and reliable, and can be used to evaluate analytic approximations.

Acknowledgments

[1] S. J. Chang, Phys. Rev. **D13**:2778-2788 (1976) [Erratum-ibid. **D16**:1979 (1977)].

[2] J. Glimm and A. Jaffe. *Quantum Physics: A Functional Integral Point of View.* Springer-Verlag, New York, 1981.

[3] Will Loinaz and R. S. Willey, Phys. Rev. **D58**:076003 (1998).

[4] U. Wolff, Phys. Rev. Lett. **62**:361-364 (1989).

[5] R. C. Brower and P. Tamayo, Phys. Rev. Lett. **62**:1087-1090 (1989).

[6] K. Binder, Z. Phys. **B43**:119 (1981).

[7] G. Parisi, Nucl. Phys. **B254**:58-70 (1985).

[8] K. Symanzik, Lett. Nuovo Cim. **8S2**:771 (1973).

[9] K. Symanzik, DESY preprint 73/58 (1973).

[10] R. Jackiw and S. Templeton, Phys. Rev. **D23**:2291-2304 (1981).

[11] R. Jackiw, Ph.D. thesis, Cornell University, 1966 (unpublished).

[12] J. M. Hauser, W. Cassing, A. Peter and M. H. Thoma, Z. Phys. **A353**:301-310 (1996).

[13] C. R. Ji, J. I. Kim, D. P. Min and A. V. Vinnikov, arXiv:hep-ph/0204114.

[14] D. Lee, Phys. Lett. **B439**:85-94 (1998).

[15] P. J. Marrero, E. A. Roura and D. Lee, Phys. Lett. **B471**:45-52 (1999).

[16] T. Sugihara, JHEP **0405**:007 (2004).

[17] C. M. Bender, S. Pinsky and B. Van de Sande, Phys. Rev. **D48**:816-821 (1993).

[18] M. Funke, U. Kaulfuss and H. Kummel, Phys. Rev. **D35**:621-630 (1987).

[19] T. Sugihara, Phys. Rev. **D57**:7373-7382 (1998).

[20] A. Harindranath and J. P. Vary, Phys. Rev. **D36**:1141-1147 (1987).

[21] A. Harindranath and J. P. Vary, Phys. Rev. **D37**:1076-1078 (1988).

[22] H. Hansen, G. Chanfray, D. Davesne and P. Schuck, Eur. Phys. J. **A14**:397-411 (2002).

[23] L. Polley and U. Ritschel, Phys. Lett. **B221**:44-48 (1989).

[24] B. Simon and R. B. Griffiths, Commun. Math. Phys. **33**:145-164 (1973).